Elastic anharmonicity of bcc Fe and Fe-based random alloys from first-principles calculations

Xiaoqing Li,[1,*] Stephan Schönecker,[2] Jijun Zhao,[3,4] Levente Vitos,[1,2,5] and Börje Johansson[1,2]

[1]*Department of Physics and Astronomy, Division of Materials Theory, Uppsala University, Box 516, SE-75120, Uppsala, Sweden*

[2]*Department of Materials Science and Engineering, Applied Materials Physics, Royal Institute of Technology, Stockholm SE-10044, Sweden*

[3]*School of Physics and Optoelectronic Technology, College of Advanced Science and Technology, Dalian University of Technology, Dalian 116024, China*

[4]*Key Laboratory of Materials Modification by Laser, Electron, and Ion Beams, Dalian University of Technology, Ministry of Education, Dalian 116024, People's Republic of China*

[5]*Research Institute for Solid State Physics and Optics, Wigner Research Center for Physics, Budapest H-1525, P.O. Box 49, Hungary*

(Received 23 August 2016; revised manuscript received 21 November 2016; published 13 January 2017)

We systematically investigate elastic anharmonic behavior in ferromagnetic body-centered cubic (bcc) Fe and $Fe_{1-x}M_x$ (M = Al, V, Cr, Co, or Ni) random alloys by means of density-functional simulations. To benchmark computational accuracy, three *ab initio* codes are used to obtain the complete set of second- and third-order elastic constants (TOECs) for bcc Fe. The TOECs of $Fe_{1-x}M_x$ alloys are studied employing the first-principles alloy theory formulated within the exact muffin-tin orbital method in combination with the coherent-potential approximation. It is found that the alloying effects on C_{111}, C_{112}, and C_{123}, which are governed by normal strains only, are more pronounced than those on C_{144}, C_{166}, and C_{456}, which involve shear strains. Remarkably, the magnitudes of all TOECs but C_{123} decrease upon alloying with Al, V, Cr, Co, or Ni. Using the computed TOECs, we study compositional effects on the pressure derivatives of the effective elastic constants (dB_{ij}/dP), bulk (dK/dP), and shear moduli (dG/dP) and derive longitudinal acoustic nonlinearity parameters (β). Our predictions show that the pressure derivatives of K and G decrease with x for all solute elements and reveal a strong correlation between the compositional trends on dK/dP and dG/dP arising from the fact that alloying predominantly alters dB_{11}/dP. The sensitivity of dB_{11}/dP to composition is attributed to intrinsic alloying effects as opposed to lattice parameter changes accompanying solute addition. For Fe and the considered Fe-based alloys, β along high-symmetry directions orders as $\beta[111] > \beta[100] > \beta[110]$, and alloying increases the directional anisotropy of β but reduces its magnitude.

DOI: 10.1103/PhysRevB.95.024203

I. INTRODUCTION

Crystal anharmonicity determines many physical properties of solids, for instance, thermal expansion, thermal conductivity, and specific heat at elevated temperatures. Anharmonicity of the lattice is also important in the discussion of crystalline imperfections, such as dislocations and interfaces, since displacements are typically large around defects. In the continuum approach, the third-order elastic constants (TOECs) are the lowest-order and most important parameters measuring anharmonicity of materials [1–3] and concerned with the nonlinear relationship between elastic strain and stress, whereas the ordinary second-order elastic constants (SOECs) characterize the linear elastic regime. In addition, TOECs serve as a basis for investigation of other anharmonic properties, e.g., the calculation of Grüneisen constants [4], the determination of cubic anharmonic force constants in studying phonon linewidths [5], and to distinguish the order of a martensitic phase transition [6]. They have also been employed to develop pseudopotentials [7] and empirical interatomic potentials [8] suitable for applications that involve relatively large displacements of atoms from equilibrium. Most recently, TOECs appeared in evaluating size effects on Young's modulus of nanowires [9].

Hitherto, the TOECs for a wide variety of bulk materials (e.g., pure metals, semiconductors, compounds, and alloys) have been determined from experiments often through ultrasound velocity measurements [1,10–12]. Less frequently, mechanical tensile testing of pristine crystalline systems, such as whiskers or nanostructures, permitted the measurement of nonlinear elastic responses at applied strains [13,14]. On the theoretical side, several approaches have been adopted to study the TOECs of single crystals, for instance, early empirical force-constant models [15,16] and molecular-dynamics simulations using fluctuation formulas [17]. Later, first-principles quantum-mechanical calculations have been employed to obtain the TOECs of various monoatomic systems and diatomic compounds [18–20]. Applications of these methods to TOECs of alloys are, however, rare.

Iron is interesting from a fundamental point of view since its thermodynamic and mechanical properties are closely related to its magnetic state [21–23]. Iron is also the main ingredient in steels, which are beyond doubt an important class of alloys and indispensable in today's industrial world. A large number of works has been dedicated to understand the alloying effect on the SOECs of pure Fe, and a detailed mapping of them as a function of composition is available today. Here, we are concerned with the investigation of TOECs for ferromagnetic body-centered cubic (bcc) Fe and the role of alloying in Fe-based alloys. We analyze and discuss other anharmonic properties that allow lending further fundamental insight into the interplay of alloying and anharmonicity in this material: (i) pressure derivatives of effective elastic constants and polycrystalline moduli, which, for example, play an important role in lattice dynamical calculations, the equation of state,

*xiaoqli@kth.se

and in studying the reversible deformation induced anisotropy in materials [24–26] and (ii) nonlinearity parameters characterizing anharmonic behavior of long-wavelength lattice vibrations. Nonlinearity parameters were linked to material damage and microstructural changes, such as fatigue [27,28], and correlated with interatomic bonding and hardness in metallic alloys [29]. It is expected that the present results are useful in studying and understanding other nonlinear phenomena in Fe-based alloys and provide a theoretical guideline for further optimizing and designing them. Since the computational determination of TOECs is a rather subtle problem, the present results can also serve as a test of both precision and accuracy in the computation of TOECs from first-principles theory.

The paper is organized as follows. In Sec. II, we briefly introduce finite-strain continuum elasticity theory, pressure derivatives of effective elastic constants and polycrystalline moduli, nonlinearity parameters, and specify details of the total energy calculations. The results are presented and discussed in Sec. III: First we assess precision and accuracy of our calculations by considering pure bcc Fe using three *ab initio* codes, and then we study the effects of five alloying elements on the TOECs of Fe. We continue with a discussion about the alloying effects on the pressure derivatives of effective effective elastic constants and polycrystalline moduli and acoustic nonlinearity parameters, which were determined from the TOECs. Finally, a conclusion of this paper is presented in Sec. IV.

II. METHODOLOGY AND COMPUTATIONAL METHOD

A. Continuum elasticity theory and methodological details

Here, we briefly introduce the basics of finite-strain elasticity theory [2,30]. Let us consider a_i to be the initial coordinates of a material point. After applying strain, the same point has new coordinates $x_i = x_i(a_j)$. The deformation applied to this material point can be measured by the deformation gradients,

$$J_{ij} = \frac{\partial x_i}{\partial a_j}, \qquad i,j = \{1 \cdots 3\}, \tag{1}$$

from which the symmetric Lagrangian strains are defined as

$$\eta_{ij} = \frac{1}{2}\sum_k (J_{ki}J_{kj} - \delta_{ij}). \tag{2}$$

In the theory of nonlinear elasticity, deformations are considered small, so it is convenient to expand the free-energy E per unit mass at 0 K as a Taylor series in terms of the strains around the equilibrium state, viz.,

$$\rho_0 E(\eta_{ij}) = \rho_0 E(0) + \frac{1}{2}\sum_{ijkl} C_{ijkl}\eta_{ij}\eta_{kl} + \frac{1}{6}\sum_{ijklmn} C_{ijklmn}\eta_{ij}\eta_{kl}\eta_{mn} + \cdots. \tag{3}$$

Here, ρ_0 is the initial mass density of the material, and $E(0)$ is the initial-state energy. C_{ijkl} and C_{ijklmn} are the second- and third-order isothermal elastic constants, respectively, evaluated at the initial state,

$$C_{ijkl} = \rho_0 \frac{\partial^2 E}{\partial\eta_{ij}\partial\eta_{kl}}\bigg|_0, \tag{4}$$

$$C_{ijklmn} = \rho_0 \frac{\partial^3 E}{\partial\eta_{ij}\partial\eta_{kl}\partial\eta_{mn}}\bigg|_0. \tag{5}$$

For a cubic crystal structure, there are three independent SOECs, C_{11}, C_{12}, and C_{44}, and six independent TOECs, C_{111}, C_{112}, C_{123}, C_{144}, C_{166}, and C_{456} (here the Voigt notation is used; $C_{\alpha\beta}$,$C_{\alpha\beta\gamma}$, where $\alpha,\beta,\gamma = \{1 \cdots 6\}$ [2]). These can be obtained by applying appropriate homogeneous Lagrangian strains [18]. In this paper, six Lagrangian strain tensors $\boldsymbol{\eta}$ were employed where the nonzero components of each strain tensor are expressed in terms of a single parameter ξ,

$$\boldsymbol{\eta}^A = \begin{pmatrix} \xi & 0 & 0 \\ 0 & 0 & 0 \\ 0 & 0 & 0 \end{pmatrix}, \quad \boldsymbol{\eta}^B = \begin{pmatrix} \xi & 0 & 0 \\ 0 & \xi & 0 \\ 0 & 0 & 0 \end{pmatrix},$$
$$\boldsymbol{\eta}^C = \begin{pmatrix} \xi & 0 & 0 \\ 0 & \xi & 0 \\ 0 & 0 & \xi \end{pmatrix}, \quad \boldsymbol{\eta}^D = \begin{pmatrix} \xi & \xi & 0 \\ \xi & 0 & 0 \\ 0 & 0 & 0 \end{pmatrix}, \tag{6}$$
$$\boldsymbol{\eta}^E = \begin{pmatrix} 0 & \xi & \xi \\ \xi & 0 & \xi \\ \xi & \xi & 0 \end{pmatrix}, \quad \boldsymbol{\eta}^F = \begin{pmatrix} \xi & 0 & 0 \\ 0 & \xi & \xi \\ 0 & \xi & 0 \end{pmatrix}.$$

The elastic energy change Eq. (3) can then be written as an expansion in the strain parameter ξ, viz.,

$$\rho_0[E(\xi) - E(0)] = \tfrac{1}{2}\lambda_2\xi^2 + \tfrac{1}{6}\lambda_3\xi^3 + \mathcal{O}(\xi^4). \tag{7}$$

The coefficient λ_2 is a combination of SOECs, and λ_3 is a combination of TOECs. The relation between these coefficients and the SOECs and TOECs for the specific strain matrices displayed above are listed in Table I. In practice, the coefficients λ_2 and λ_3 may be obtained by fitting Eq. (7) to calculated energy-strain data for each $\boldsymbol{\eta}$, and consequently the full set of SOECs and TOECs can be derived. We found that the obtained λ_2 for the SOECs were not sensitive to the strain range of fitting. However, the coefficient λ_3 was more sensitive to the maximum ξ. Our results showed that the TOECs converged for the maximum strain parameter $|\xi|$ larger than a certain value and were stable over a certain range, e.g., the variations of the TOECs C_{111} and C_{456} were $<2\%$ when

TABLE I. The relations between the coefficients λ_2 and λ_3 in Eq. (7) and the second- and third-order elastic constants for the Lagrangian strain tensors $\boldsymbol{\eta}$ specified in Eq. (6).

$\boldsymbol{\eta}$	λ_2	λ_3
$\boldsymbol{\eta}^A$	C_{11}	C_{111}
$\boldsymbol{\eta}^B$	$2C_{11} + 2C_{12}$	$2C_{111} + 6C_{112}$
$\boldsymbol{\eta}^C$	$3C_{11} + 6C_{12}$	$3C_{111} + 18C_{112} + 6C_{123}$
$\boldsymbol{\eta}^D$	$C_{11} + 4C_{44}$	$C_{111} + 12C_{166}$
$\boldsymbol{\eta}^E$	$12C_{44}$	$48C_{456}$
$\boldsymbol{\eta}^F$	$2C_{11} + 2C_{12} + 4C_{44}$	$3(2C_{111}/3 + 2C_{112} + 4C_{144} + 4C_{166})$

$|\xi|$ was changed from 0.08 to 0.10. Therefore, in this paper, ξ was varied between -0.09 and 0.09 with step 0.01.

Applied homogeneous strains distort the crystal lattice. In order to construct the deformed crystal structure spanned by a basis lattice vector $\boldsymbol{r}'$ from the unstrained configuration, the deformation gradients J_{ij} are applied to an unstrained basis lattice vector $\boldsymbol{r}$ as in Ref. [18], viz.,

$$r_i' = \sum_j J_{ij} r_j. \tag{8}$$

We may obtain the deformation gradients J_{ij} from the Lagrangian strains η_{ij} by inverting Eq. (2).

B. Pressure derivatives of effective elastic constants and polycrystalline moduli

The relation between the variation of stress and the variation of strain of a loaded crystal has been the focus of several theoretical works [2,30–35]. Accordingly, the effective elastic constants B_{ijkl} (sometimes referred to as Birch coefficients or stress-strain coefficients in the literature) are particularly useful for the analysis of crystals under isotropic pressure. For the sake of a self-contained work, their relation to the second-order coefficients C_{ijkl} under arbitrary pressure P is given in Appendix A.

Following Birch [31] and Wallace [2,30], the $B_{\alpha\beta}$ (Voigt notation) may be expanded in a Taylor series around the equilibrium state, and for linear order in P we have

$$B_{\alpha\beta}(P) = B_{\alpha\beta}\Big|_0 + \frac{dB_{\alpha\beta}}{dP}\Big|_0 P + \mathcal{O}(P^2). \tag{9}$$

The $\frac{dB_{\alpha\beta}}{dP}$ are the first-order pressure derivatives evaluated at zero pressure expressed in terms of SOECs and TOECs, which for cubic symmetry read (Appendix B)

$$\frac{dB_{11}}{dP} = -\frac{2(C_{11}+C_{12})+C_{111}+2C_{112}}{C_{11}+2C_{12}}, \tag{10a}$$

$$\frac{dB_{12}}{dP} = -\frac{-C_{11}-C_{12}+2C_{112}+2C_{123}}{C_{11}+2C_{12}}, \tag{10b}$$

$$\frac{dB_{44}}{dP} = -\frac{C_{11}+2C_{12}+C_{44}+C_{144}+2C_{166}}{C_{11}+2C_{12}}, \tag{10c}$$

$$\frac{dB'}{dP} = \frac{1}{2}\left(\frac{dB_{11}}{dP} - \frac{dB_{12}}{dP}\right). \tag{10d}$$

We defined $B' = (B_{11} - B_{12})/2$. It should be noted that $B_{\alpha\beta} = C_{\alpha\beta}$ at zero pressure (Appendix A).

With the help of Eqs. (10a)–(10d), we may obtain the pressure derivatives of the polycrystalline shear $\frac{dG}{dP}$ and bulk $\frac{dK}{dP}$ moduli at arbitrary pressure P [33]. Here, the values of $\frac{dG}{dP}$ were computed using the Hill average method for G [36] in order to facilitate comparison with measured polycrystalline data. We obtain

$$\frac{dK}{dP} = \frac{1}{3}\left(\frac{dB_{11}}{dP} + 2\frac{dB_{12}}{dP}\right), \tag{11a}$$

$$\frac{dG}{dP} = \frac{1}{2}\left(\frac{dG_R}{dP} + \frac{dG_V}{dP}\right), \tag{11b}$$

$$\frac{dG_V}{dP} = \frac{1}{5}\left(\frac{dB_{11}}{dP} - \frac{dB_{12}}{dP} + 3\frac{dB_{44}}{dP}\right), \tag{11c}$$

$$\frac{dG_R}{dP} = \frac{5\left(\frac{dB'}{dP}B_{44} + \frac{dB_{44}}{dP}B'\right) - \left(2\frac{dB_{44}}{dP} + 3\frac{dB'}{dP}\right)G_R}{2B_{44}+3B'}, \tag{11d}$$

where

$$G_R = \frac{5B'B_{44}}{2B_{44}+3B'}. \tag{12}$$

C. Nonlinearity parameters

The deviation of a solid from linear stress-strain behavior has been quantified using nonlinearity parameters by many researchers [37–39]. In this paper, a proposed generalized definition of the acoustic nonlinearity parameters β for single crystals is employed [37]

$$\beta = -\frac{\sum_{ijklmn}(C_{jlmn}\delta_{ik} + C_{ijnl}\delta_{km} + C_{jknl}\delta_{im} + C_{ijklmn})\hat{n}_j\hat{n}_l\hat{n}_n\hat{u}_i\hat{u}_k\hat{u}_m}{\sum_{ijkl} C_{ijkl}\hat{n}_j\hat{n}_l\hat{u}_i\hat{u}_k}, \tag{13}$$

where $\hat{\boldsymbol{n}}$ and $\hat{\boldsymbol{u}}$ are the wave propagation and polarization directions (normalized to unity), respectively. The longitudinal acoustic nonlinearity parameters for a cubic crystal in the high-symmetry [100], [110], and [111] directions are the most important ones, viz.,

$$\beta[100] = -\left(3 + \frac{C_{111}}{C_{11}}\right), \tag{14a}$$

$$\beta[110] = -\left(3 + \frac{C_{111}+3C_{112}+12C_{166}}{2(C_{11}+C_{12}+2C_{44})}\right), \tag{14b}$$

$$\beta[111] = -\left(3 + \frac{C_{111}+6C_{112}+12C_{144}+24C_{166}+2C_{123}+16C_{456}}{3(C_{11}+2C_{12}+4C_{44})}\right). \tag{14c}$$

D. Total energy calculation

In this paper, the employed *ab initio* approach is based on density-functional theory [40]. The generalized-gradient approximation of the Perdew-Burke-Ernzerhof [41] functional was adopted to describe exchange and correlation, which is well known to give the correct ferromagnetic bcc ground state for Fe. For the main part of the paper, the Kohn-Sham equations were solved using the exact muffin-tin orbital (EMTO) method [42,43]. The scalar relativistic approximation and the soft core scheme were used. Brillouin-zone integrations were performed on a $33 \times 33 \times 33$ uniform k mesh. The problem of chemical disorder in $Fe_{1-x}M_x$ alloys was treated within the coherent-potential approximation (CPA), and the total energy was computed via the full charge-density technique [44–46]. Since the CPA is a single-site approximation, local lattice relaxation (LLR) was not accounted for in the present paper. Recent investigations for random Ti-Al and Cu-Au alloys showed that LLR has a minor effect on SOECs for low solute concentration ($\lessapprox 15$ at. %) [47]. This result is in agreement with the work of Zhang *et al.* for the presently considered $Fe_{1-x}M_x$ binaries [48], who reported that the LLR effect on the lattice parameter and bulk modulus for Fe-rich binaries ($x = 0.0625$) is small. Thus, we expect that LLR has a negligible effect on the SOECs and TOECs for the present considered $Fe_{1-x}M_x$ alloys where the maximum solute concentration is 0.1. The accuracy of the EMTO method for the equation of state and SOECs of metals and alloys (including Fe-based alloys) was demonstrated in a number of previous works [48–50] and is assessed for the TOECs of Fe in Sec. III A.

Additional calculations for pure Fe were performed with the full-potential local-orbital (FPLO) scheme FPLO-14 [51], and the projector-augmented wave (PAW) method as implemented in the Vienna *ab initio* simulation package (VASP) release 5.3.3 [52]. The FPLO calculations were performed in the scalar-relativistic approximation. Convergence of the numerical parameters, in particular integration meshes and the basis, was carefully checked. Linear-tetrahedron integrations with Blöchl corrections were performed on a $48 \times 48 \times 48$ mesh in the full Brillouin zone and the valence basis contained $3d$, $4spd$, and $5s$ states. All VASP calculations were performed with the default spd-valence state PAW potential and the global "accurate" precision switch. Total energies were found converged for a plane-wave cutoff of 500 eV. Brillouin-zone integrations were performed on a $33 \times 33 \times 33$ Monkhorst-Pack mesh, smeared by a first-order Methfessel-Paxton scheme with a smearing parameter of 0.1 eV. The grid for augmentation charges contained eight times more points than the default.

We should emphasize that the FPLO and VASP calculations involve full Kohn-Sham potentials, whereas the EMTO method is based on the optimized overlapping muffin-tin (OOMT) approximation. Furthermore, the FPLO method uses local orbitals as basis functions in contrast to the plane waves used in the PAW and the partial waves in the EMTO. Hence, comparing the three sets of *ab initio* results for pure Fe helps to assess the accuracy of the OOMT approximation as well as the basis set dependence of the predicted properties.

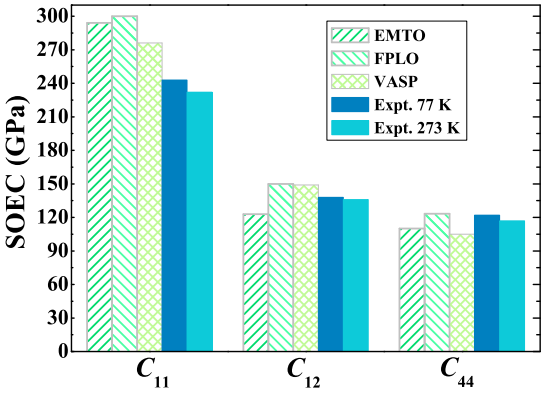

FIG. 1. The three independent SOECs of bcc ferromagnetic Fe computed from non-volume-conserving Lagrangian strains. The present results (EMTO, FPLO, and VASP) are compared with available experimental data from Ref. [56].

III. RESULTS AND DISCUSSIONS

A. Second- and third-order elastic constants of bcc iron

Our methodological approach permits the simultaneous determination of the second- and third-order elastic constants in the framework of finite-strain elasticity theory. On the other hand, SOECs may be extracted from energy-strain or stress-strain relationships using the infinitesimal-strain formalism for which we use the notation c_{ijkl} for clarity, where

$$c_{ijkl} = \rho_0 \frac{\partial^2 E}{\partial e_{ij} \partial e_{kl}}\bigg|_0, \tag{15}$$

and e_{ij} is the Eulerian strain tensor. In the following we use Voigt notation ($c_{\alpha\beta}$). Before turning to the TOECs, we briefly discuss and compare the results of both approaches to the SOECs for bcc Fe.

We show the SOECs of bcc Fe obtained from the strains $\boldsymbol{\eta}^A$, $\boldsymbol{\eta}^B$, and $\boldsymbol{\eta}^E$ using the EMTO, FPLO, and VASP methods and available experimental data in Fig. 1. It can clearly be seen that the three *ab initio* codes systematically overestimate C_{11} but yield C_{12} and C_{44} in reasonable agreement with the low-temperature experimental values [53]. These theoretical data are compared (Table II) to the results employing infinitesimal-strain elasticity theory and volume-conserving strains in the determination of c_{44} and $c' = (c_{11} - c_{12})/2$ as detailed in Ref. [54] in addition to deriving the linear combination $c_{11} + 2c_{12} = 3K$ from the equation of state (K denotes the bulk modulus). We find that the largest systematic deviation occurs between C_{44} and c_{44}, and C_{12} (c_{12}) from the

TABLE II. The three independent SOECs (in units of gigapascals) of bcc Fe obtained from the infinitesimal-strain formalism ($c_{\alpha\beta}$) and the non-volume-conserving Lagrangian strains ($C_{\alpha\beta}$).

Method	c_{11}	C_{11}	c_{12}	C_{12}	c_{44}	C_{44}
EMTO	287	292	132	123	106	110
FPLO	297	300	150	150	117	123
VASP	278	276	149	149	100	105

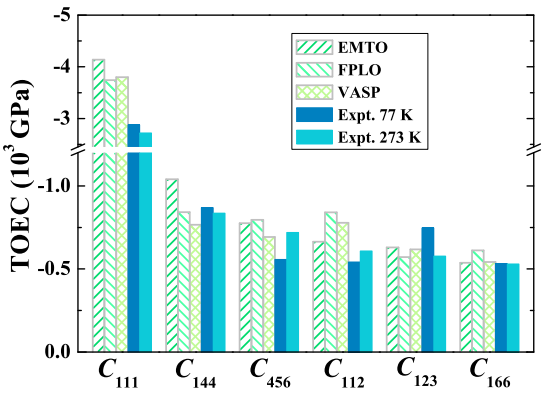

FIG. 2. The six independent TOECs of bcc ferromagnetic Fe. The present results (EMTO, FPLO, and VASP) are compared with available experimental data from Ref. [56].

EMTO is somewhat sensitive to the approach. Nevertheless, the results derived from the infinitesimal-strain and the non-volume-conserving Lagrangian strain formalisms are overall in close agreement with each other.

The scatter of the theoretical data apparent from Fig. 1 may be taken as a measure of the typical precision presently achievable in calculations of the SOECs of Fe across different all-electron schemes. A plausible explanation for part of the systematic deviation of C_{11} from the experimental value is the underestimation of the equilibrium volume (a detailed comparison of equilibrium lattice parameters of Fe can be found in Ref. [55]). We may use the relation $dC_{11}/dV = dC_{11}/dP \times dP/dV$ to see that the deviation of C_{11} by underestimating the volume is proportional to the pressure derivative of C_{11} (P denotes the pressure). dC_{11}/dP turns out to be the largest among the pressure derivatives of SOECs of Fe (see Sec. III C and Appendix A), suggesting why C_{11} has the largest error.

Figure 2 displays the six independent TOECs of bcc Fe from our calculations and available experimental data [56]. As is evident, all six TOECs obtained from the three *ab initio* codes are negative, and C_{111} is significantly larger in magnitude compared to the other five TOECs. This is in good agreement with the experimental data [56]. The values obtained from the different numerical methods show common features, such as all of them systematically overestimate $|C_{111}|$, $|C_{112}|$, and $|C_{456}|$, underestimate $|C_{123}|$ but give good C_{144} and C_{166}, compared with the experimental data at 77 K.

In order to further evaluate the performance of the three *ab initio* codes for the TOECs, we studied the mean absolute relative deviations (MARDs) of the calculated values from the measured data at 77 K. The obtained MARDs are approximately 24%, 27%, and 22% for the EMTO, FPLO, and VASP, respectively, which correspond to 2–5% scatter among the numerical methods. When comparing *ab initio* results to experimental data, it should be mentioned that the above *ab initio* calculations were performed for a perfect crystalline structure at 0 K, whereas the measurements were carried out at finite temperatures on samples that often contain defects. Furthermore, due to difficulties in the experimental procedure, reported TOECs typically exhibit relative uncertainties exceeding those of SOECs [10]. On the theoretical side, despite careful convergence of numerical parameters, the exchange-correlation approximation may always be one possible source for the discrepancy. Thus, keeping the above in mind together with our assessments, we conclude that the EMTO, FPLO, and VASP describe the TOECs of bcc FM Fe well, which provides the support for the approach used in this paper, and continue with Fe-based alloys.

B. Second- and third-order elastic constants of bcc Fe-based alloys

Using the EMTO method, we investigated the TOECs of $Fe_{1-x}M_x$ random solid solutions, where M = Al, V, Cr, Co, or Ni. The selected solute atoms commonly are used alloying elements in commercial Fe-based steels. The concentration of the solutes x was varied from 0 to 10 at. %. Because the evaluation of pressure derivatives and nonlinearity parameters (Secs. III C and III D) also requires the knowledge of the SOECs of the alloys, we present them here for the sake of completeness. Here, all SOECs were obtained in the framework of finite-strain elasticity theory using $\boldsymbol{\eta}^A$, $\boldsymbol{\eta}^B$, and $\boldsymbol{\eta}^E$.

Figure 3 shows the calculated SOECs and TOECs of Fe as a function of alloying concentration. We find that the predicted alloying trend of the SOECs overall agree well with results of a previous study [48] using the infinitesimal-strain formalism. We refer the reader to Refs. [48,57] for a more detailed discussion of the alloying effects on the SOECs.

For all binaries considered here, the obtained TOECs are negative. As can be seen, C_{111}, C_{112}, and C_{123} are particularly sensitive to the solute concentration. These three elastic constants are governed by normal strains only. The magnitudes of C_{111} and C_{112} decrease with increasing alloying concentration in contrast to C_{123}, whose magnitude increases. On the other hand, the three elastic constants also involving shear strains, C_{144}, C_{166}, and C_{456}, are relatively insensitive to alloy concentration and just slightly decrease with increasing alloying content. Co shows the weakest compositional effect on several TOECs, but Ni turns out to have the strongest effect on several TOECs, such as for C_{111}, which reduces by $\sim$11% and $\sim$35% when 10% Co and 10% Ni, respectively, are added to Fe.

C. Pressure derivatives of effective elastic constants and polycrystalline moduli of bcc Fe and Fe-based alloys

The pressure derivatives of the coefficients $B_{\alpha\beta}$ and polycrystalline moduli for pure Fe obtained in this paper using the three *ab initio* codes, those derived here from available experimental SOECs and TOECs at 77 and 273 K and using the Hill average for G, as well as the reported measurements are given in Table III. We find that the values computed with the three *ab initio* codes are in close agreement with each other. On one hand, all methods consistently overestimate $\frac{dB_{11}}{dP}$ and, as a result, yield too large $\frac{dB'}{dP}$ compared to the experimental data. We attribute these differences to the overestimation of $|C_{111}|$ by all three *ab initio* codes (see Fig. 2). To underline this point, if the computed C_{111} equaled the experimental value at 77 K from Ref. [56] (and the other calculated TOECs unchanged), the pressure derivatives of B_{11} and B' by the EMTO would decrease to 6.4 and 1.0, respectively, bringing

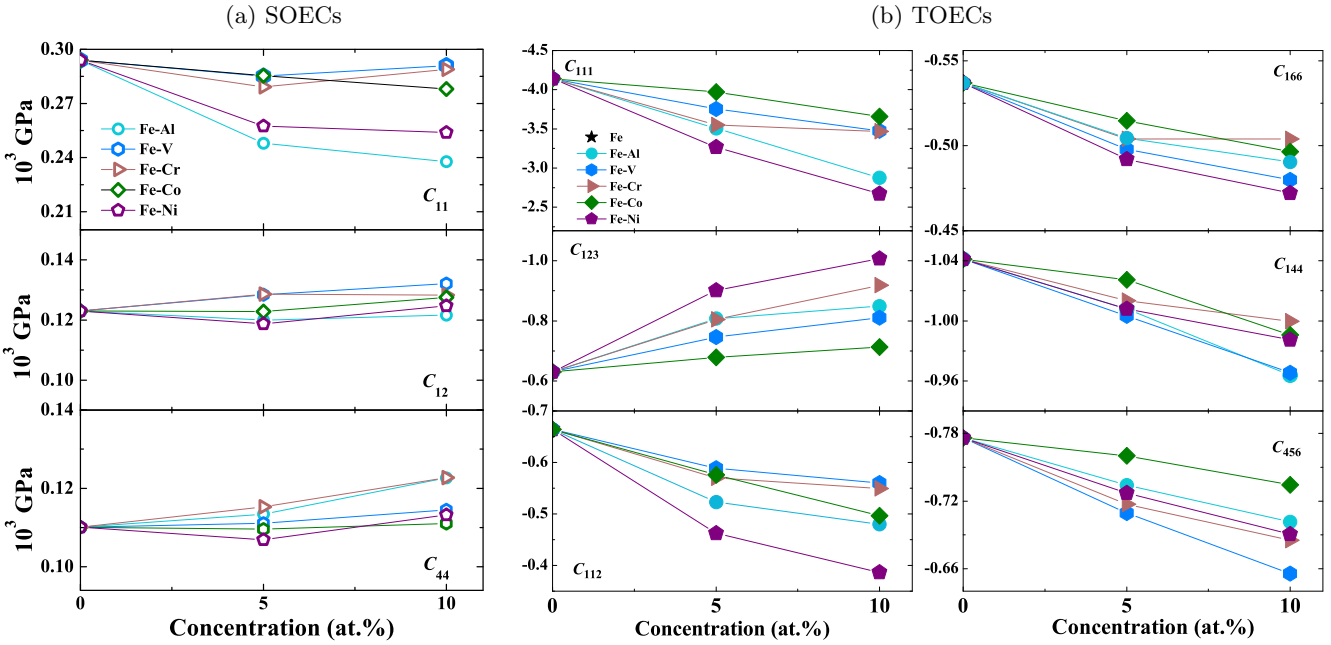

FIG. 3. The three independent SOECs and six independent TOECs of $Fe_{1-x}M_x$ alloys as a function of solute concentration x. All elastic constants are in units of 10^3 GPa.

them very close to the experimental data. On the other hand, the results for the pressure derivative of B_{12} and B_{44} agree well with those derived from the experimental SOECs and TOECs [53,56] and measurements [58,59]. The pressure derivatives of the bulk and shear moduli obtained from the three *ab initio* codes are close to each other and in good agreement with the measured data [58–60] but larger than those determined from the experimental SOECs and TOECs [53,56].

An alternative theoretical approach that does not involve TOECs may be employed to determine the pressure derivatives of $B_{\alpha\beta}$. Accordingly, one fits the linear function Eq. (9) to computed $B_{\alpha\beta}$ as a function of P (cf. Appendix A). Without loss of generality, we used the EMTO to estimate $\frac{dB_{\alpha\beta}}{dP}$ in this way and list the results in parentheses in Table III. The two sets of theoretical data are in good agreement, i.e., $\frac{dB_{11}}{dP}$ is slightly smaller, and both $\frac{dB_{12}}{dP}$ and $\frac{dB_{44}}{dP}$ are slightly larger than the values involving TOECs [Eqs. (10a)–(10d)]. The resulting two sets for $\frac{dK}{dP}$ and $\frac{dG}{dP}$ are in close agreement as well. We do not find a general improvement with respect to the experimental values. This finding supports the robustness of our predictions and points towards the above discussed overestimation of C_{111} as one of the main reasons behind the differences seen in Table III between the theoretical and the experimental values.

The detailed analysis of the compositional effects on the pressure derivatives of bulk and shear moduli for bcc Fe is given in Fig. 4. We find that $\frac{dK}{dP}$ of Fe decreases with any considered alloying addition. Ni shows the strongest alloying effect, whereas Co overall has the weakest one. For example, adding 10 at. % Ni into Fe reduced $\frac{dK}{dP}$ of Fe by nearly 20%. Surprisingly, the alloying trend on $\frac{dG}{dP}$ is very similar to that of $\frac{dK}{dP}$ as shown in Fig. 4. Accordingly, the anharmonic response of both the bulk modulus and the shear modulus due to external hydrostatic pressure reduces as a result of adding Al, V, Cr, Co, or Ni to bcc Fe. The correlation between $\frac{dK}{dP}$ and $\frac{dG}{dP}$ for the considered $Fe_{1-x}M_x$ alloys approximately obeys the following

TABLE III. The pressure derivative of the effective elastic constants $B_{\alpha\beta}$ and polycrystalline moduli from our calculations, derived from available experimental SOECs and TOECs [53,56] at 77 and 273 K as well as from measurements [58–60] at 300 K for pure Fe. The values in parentheses were obtained from SOECs evaluated under pressure; see the text for details.

Method	$\frac{dB_{11}}{dP}$	$\frac{dB_{12}}{dP}$	$\frac{dB_{44}}{dP}$	$\frac{dB'}{dP}$	$\frac{dK}{dP}$	$\frac{dG}{dP}$
EMTO	8.6 (8.4)	4.4 (5.2)	2.7 (3.2)	2.1 (1.6)	5.8 (6.3)	2.4 (2.5)
FPLO	7.7	4.4	2.3	1.7	5.5	2.0
VASP	8.0	4.5	2.3	1.8	5.6	2.0
Expt. 77 K (Refs. [53,56])	6.2	4.3	2.5	1.0	4.9	1.7
Expt. 273 K (Refs. [53,56])	6.4	4.4	2.5	1.0	5.0	1.8
Expt. 300 K (Ref. [58])	6.8	4.6	2.6	1.1	5.3	1.8[a]
Expt. 300 K (Ref. [59])	6.4	5.2	2.7	1.2	6.0	1.9[a]
Expt. 300 K (Ref. [60])					5.1	2.2[b]

[a]Measurement on a single crystal. Polycrystalline data from the Hill average.
[b]Measurement on a polycrystal.

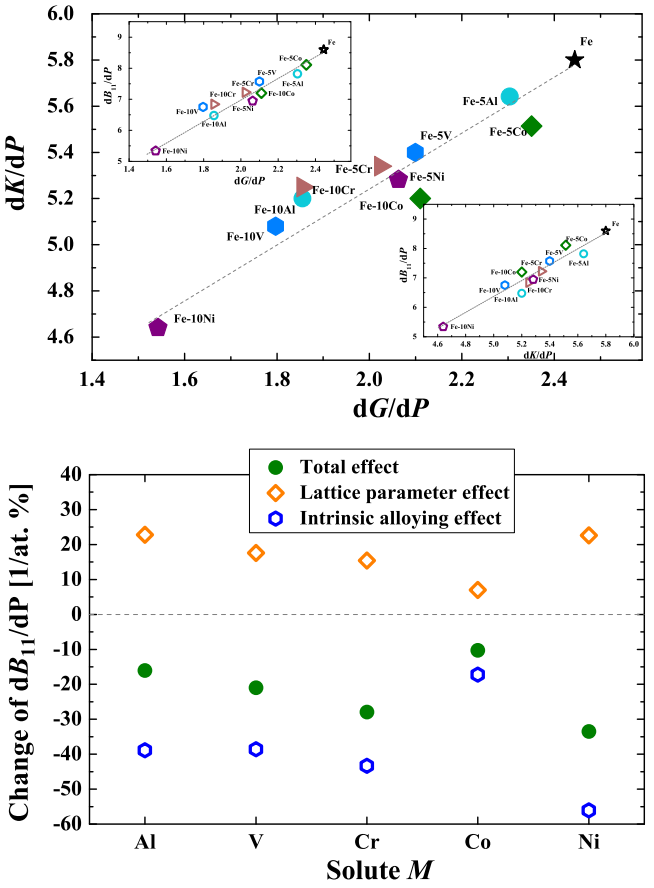

FIG. 4. (a) Correlation between the pressure derivatives of the bulk modulus and the shear modulus for $Fe_{1-x}M_x$ alloys (x denotes the concentration of solute M, $x \leqslant 0.1$). The dashed line is a linear fit to the data (for details see the text). The insets display the correlation between the pressure derivatives of B_{11} and the shear and bulk moduli. (b) The total effect on dB_{11}/dP evaluated by means of a finite concentration change $\Delta x = 0.05$ with pure Fe as a reference and the decomposition into the lattice parameter effect and the intrinsic alloying effect according to Eq. (17).

linear relationship:

$$\frac{dK}{dP} = 0.98\frac{dG}{dP} + 3.4, \tag{16}$$

which also is indicated in Fig. 4.

To seek the primary reason behind the linear relationship Eq. (16), we consult the compositional effect on the individual pressure derivatives. We find that the alloying effects on $\frac{dB_{12}}{dP}$ and $\frac{dB_{44}}{dP}$ are significantly weaker *on average* than the one on $\frac{dB_{11}}{dP}$. We may hence consider the former two to be constant (equal to the values of pure iron) in the following brief analysis. The compositional effect on $\frac{dK}{dP}$ then is determined mainly by the alloying effect on $\frac{dB_{11}}{dP}$ and approximately follows a simple linear relationship; see the lower inset of Fig. 4(a). By the same reasoning, the compositional effect on $\frac{dG_V}{dP}$ is mainly controlled by that on $\frac{dB_{11}}{dP}$ also approximately obeying a linear relationship [Eq. (11c)]. Since $\frac{dG_R}{dP}$ typically scales with $\frac{dG_V}{dP}$ (the former is a lower bound, and the latter is an upper bound), a linear correlation between the compositional effect on their arithmetic average $\frac{dG}{dP}$ [Eq. (11b)] and the one on $\frac{dB_{11}}{dP}$ can be expected. That this is indeed the case is demonstrated in the upper inset of Fig. 4(a) based on the actual computed values for $\frac{dG}{dP}$ and $\frac{dB_{11}}{dP}$. We conclude from this analysis that the dominant alloying effect on $\frac{dB_{11}}{dP}$ is the primary reason behind the linear correlation Eq. (16).

In an attempt to understand the alloying effect on the pressure derivative of B_{11}, we separate the changes caused by the intrinsic alloying effect (electronic structure) at isovolumetric conditions from that due to the lattice parameter change accompanying solute addition. Thus, we assume that $\frac{dB_{11}}{dP}$ is a function of the alloying concentration x and the lattice parameter a, i.e., $\frac{dB_{11}}{dP}(x,a(x))$. The total change in $\frac{dB_{11}}{dP}$ with x may be written as

$$\frac{d(dB_{11}/dP)}{dx} = \left(\frac{\partial(dB_{11}/dP)}{\partial x}\right)_a + \left(\frac{\partial(dB_{11}/dP)}{\partial a}\right)_x \frac{da}{dx}. \tag{17}$$

Pure Fe was selected as the reference state. The first term on the right-hand side of Eq. (17) is the intrinsic alloying effect with respect to a change in alloy concentration at a constant lattice parameter (equilibrium lattice parameter of bcc Fe). Since for alloys the equilibrium lattice parameter depends on the concentration, dB_{11}/dP is evaluated at that particular pressure that brings the volume of the $Fe_{1-x}M_x$ alloy in coincidence with the equilibrium volume of pure Fe. The second term on the right-hand side of Eq. (17) measures the lattice parameter effect at constant concentration (pure Fe; $x = 0$) multiplied by the change in the equilibrium lattice parameter accompanying alloying ($\frac{da}{dx}$). This term reflects the change in dB_{11}/dP of pure Fe evaluated at that particular pressure that brings the volume of bcc Fe in coincidence with the equilibrium volume of $Fe_{1-x}M_x$.

In practice, the total effect was evaluated by means of a finite concentration change $\Delta x = 0.05$ from the data shown in the inset of Fig. 4(a) with pure Fe as the reference state. The lattice parameter effect was estimated from an analytical model for $B_{11}(P)$ as detailed in Appendix B. The intrinsic alloying effect was defined as to balance Eq. (17). It should be noted that previous numerical simulations predict that all presently considered solutes (and $x = 0.05$) increase the equilibrium lattice parameter of bcc Fe [55], and we refer the reader to that paper for a more detailed presentation and discussion.

TABLE IV. The longitudinal acoustic nonlinearity parameters of bcc Fe in the [100], [110], and [111] directions. The values determined from experimental SOECs [53] and TOECs [56] are listed for comparison.

Method	β[100]	β[110]	β[111]
EMTO	11.1	6.9	13.0
FPLO	9.4	7.0	11.6
VASP	10.7	7.1	11.5
Expt. 77 K (Refs. [53,56])	8.8	5.7	10.2
Expt. 273 K (Refs. [53,56])	8.7	6.1	11.4

TABLE V. The longitudinal acoustic nonlinearity parameters of $Fe_{1-x}M_x$ alloys as a function of concentration.

M	x	β[100]	β[110]	β[111]
Al	0.05	11.0	6.4	12.3
	0.1	9.1	5.4	11.4
V	0.05	10.2	6.0	11.9
	0.1	8.9	5.4	10.8
Cr	0.05	9.7	5.9	11.8
	0.1	9.0	5.4	11.0
Co	0.05	10.9	6.5	12.7
	0.1	10.2	5.8	11.9
Ni	0.05	9.7	5.9	12.7
	0.1	7.5	4.8	11.4
Range of β:		7.5–11.0	4.8–6.5	10.8–12.7

With the results given in Fig. 4(b), we are able to estimate the intrinsic alloying effect and the lattice parameter effect on $\frac{dB_{11}}{dP}$ for adding 5 at. % solute to pure Fe. One can see that the lattice parameter effects are all positive and the intrinsic alloying effects turn out to be all negative. In other words, the intrinsic alloying effect is the main driving force for the observed changes in the pressure derivative of B_{11}, whereas the lattice parameter effect gives a smaller correction. The trend of the lattice parameter effect can be understood since all considered solutes expand the lattice parameter of Fe (Ref. [55]), and the second derivative of B_{11} with respect to P of Fe is a monotonically decreasing function in P (Appendix B). In other words, the larger the compositional effect on the equilibrium lattice parameter, the larger the change in dB_{11}/dP. The total effect in Fig. 4(b) is set by the concentration dependencies of the SOECs and TOECs (Sec. III B). For dB_{11}/dP, C_{111} plays the most important role as it is the elastic constant that experiences the largest changes with composition, e.g., alloying with Co (Ni) leads to the weakest (strongest) compositional effect on C_{111} in accordance with the trend seen in Fig. 4(b).

D. Nonlinearity parameters of bcc Fe and Fe-based alloys

Results for the acoustic nonlinearity parameters of bcc Fe obtained from the presently computed elastic constants are presented in Table IV together with data determined from experimental SOECs and TOECs. We can see that the calculated nonlinearity parameters along the three special directions are larger than those obtained from the experimental elastic constants, however, they are still in good agreement. Furthermore, we observe that the nonlinearity parameters order as $\beta[111] > \beta[100] > \beta[110]$, i.e., longitudinal elastic anharmonicity is the largest along the [111] direction.

The concentration dependence of the nonlinearity parameters for the present binary alloys is shown in Table V. It is found that the nonlinearity parameters of Fe for the three considered directions decrease with x for each solute. The nonlinearity parameters in the [100] and [110] directions show pronounced compositional effects with maximum changes of 32.4% and 30.0% for $x = 0.1$, respectively, whereas alloying has a weaker effect on the nonlinearity parameter of Fe in the [111] direction (a variation of 16.9%). The obtained results indicate that anharmonic corrections to long-wavelength acoustic lattice modes diminish in all three high-symmetry directions with introducing any of the considered alloying elements to Fe. In other words, the response to interatomic displacements becomes more symmetric with respect to positive or negative elongations. This effect is most noticeable in the [100] and [110] directions. Interestingly, solute addition does not influence the directional ordering of the nonlinearity parameters, i.e., $\beta[111] > \beta[100] > \beta[110]$ holds for all considered Fe-based alloys.

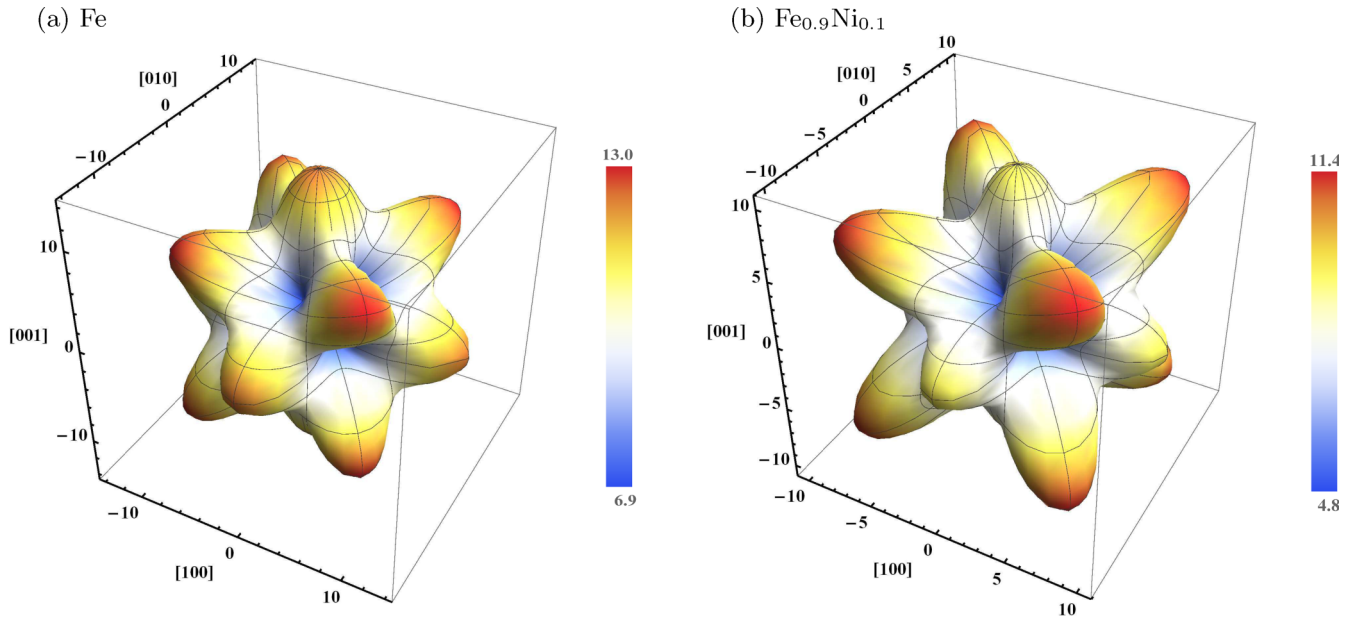

FIG. 5. The longitudinal acoustic nonlinearity parameter β as a function of wave propagation direction for (a) bcc Fe and for (b) a $Fe_{0.9}Ni_{0.1}$ alloy. The Cartesian axes specify the projection of β onto the [100], [010], and [001] crystallographic axes.

To illustrate the full directional dependence of the longitudinal acoustic nonlinearity parameter, we show β as a function of wave propagation direction for pure Fe and for $Fe_{0.9}Ni_{0.1}$ (as an example for the alloys) in Fig. 5. Although β decreases with alloying Ni, the anisotropy of β (ratio of largest values to smallest value $\beta[111]/\beta[110]$) increases in fact. This is true for any of the considered solutes.

IV. CONCLUSIONS

We presented a detailed first-principles investigation of elastic anharmonicity in bcc Fe and Fe-based random alloys. Three *ab initio* codes (the EMTO, FPLO, and VASP) were employed to systematically benchmark the TOECs $C_{\alpha\beta\gamma}$ of Fe. In possession of the $C_{\alpha\beta\gamma}$, we also assessed the pressure derivatives of Birch's effective SOECs $dB_{\alpha\beta}/dP$ and the longitudinal acoustic nonlinearity parameters β. Although the computational determination of TOECs is subtle, it is encouraging that the three *ab initio* codes yield comparable results. The obtained values for Fe are in good agreement with available experimental data; solely C_{111} is noticeably underestimated by the three *ab initio* codes, and this error propagates to the pressure derivatives of B_{11} and B'.

Using the EMTO method in combination with the coherent-potential approximation, we investigated the TOECs of bcc $Fe_{1-x}M_x$ (M = Al, V, Cr, Co, or Ni) random alloys for $x \leqslant 0.1$. The alloying effects on C_{111}, C_{112}, and C_{123} turned out to be stronger than those on C_{144}, C_{166}, and C_{456}. Remarkably, the magnitudes of all TOECs but C_{123} decrease upon alloying with Al, V, Cr, Co, or Ni indicating a predominantly diminished anharmonic contribution to the elastic stress-strain relationship for the binaries. With the help of additionally obtained SOECs, we showed that the pressure derivatives of the polycrystalline bulk and shear moduli (K and G, respectively) decrease with x for all solute elements and established a linear correlation between the compositional effects on dK/dP and dG/dP. The dominant effect behind this linear correlation is the strong variation of dB_{11}/dP with x as opposed to dB_{12}/dP and dB_{44}/dP. To shed light on the alloying effect on dB_{11}/dP, we disentangled the intrinsic (electronic) alloying effect at isovolumetric conditions from that due to the lattice parameter change accompanying solute addition. The former turned out to prevail in all cases. The computed nonlinearity parameters for long-wavelength longitudinal acoustic modes in high-symmetry directions were found to order as $\beta[111] > \beta[100] > \beta[110]$ in bcc Fe and $Fe_{1-x}M_x$ indicating the largest degree of anharmonicity in the [111] direction. Alloying with any of the considered solutes generally increases the directional anisotropy of β but reduces its magnitude. The latter suggests overall diminished longitudinal acoustic phonon anharmonicities in the long-wavelength limit.

Our results may serve as a guide and useful reference for scientists who would further study and understand the anharmonic properties of Fe-based alloys. For instance, recently proposed nondestructive testing techniques based on nonlinear ultrasound have been used to characterize microstructural changes in metallic materials, such as fatigue or radiation damage [61–63]. These exploit the link between the amplitude of second harmonics generated by the propagation of incident longitudinal waves and the material's SOECs and TOECs as well as dislocation density.

ACKNOWLEDGMENTS

The Carl Tryggers Foundation for Scientific Research, the Swedish Research Council, the Swedish Steel Producers' Association, the Swedish Foundation for Strategic Research, the Swedish Foundation for International Cooperation in Research and Higher Education, the Hungarian Scientific Research Fund (Research Project No. OTKA 109570), and the National Magnetic Confinement Fusion Program of China (Grant No. 2015GB118001) are acknowledged for financial support. The simulations were performed on resources provided by the Swedish National Infrastructure for Computing (SNIC) at the National Supercomputer Centre in Linköping.

APPENDIX A: RELATIONSHIP BETWEEN SECOND-ORDER COEFFICIENTS UNDER PRESSURE

The relations between the effective SOECs (B_{ijkl}) and the second derivatives of the free energy taken with respect to Lagrangian strain parameters (C_{ijkl}) or infinitesimal-strain variables (c_{ijkl}) *under arbitrary isotropic pressure* P are given by the following equations [2,30–32]:

$$B_{ijkl} = C_{ijkl} + P(\delta_{ij}\delta_{kl} - \delta_{il}\delta_{jk} - \delta_{ik}\delta_{jl}), \quad \text{(A1a)}$$

$$B_{ijkl} = c_{ijkl} + \tfrac{1}{2}P(2\delta_{ij}\delta_{kl} - \delta_{il}\delta_{jk} - \delta_{ik}\delta_{jl}). \quad \text{(A1b)}$$

For a crystal with cubic symmetry (Laue group I), the relations for the three independent second-order coefficients are as follows for arbitrary P:

$$B_{1111} = C_{1111} - P = c_{1111}, \quad \text{(A2a)}$$

$$B_{1122} = C_{1122} + P = c_{1122} + P, \quad \text{(A2b)}$$

$$B_{2323} = C_{2323} - P = c_{2323} + \tfrac{1}{2}P. \quad \text{(A2c)}$$

The relations between the pressure derivatives of the second-order coefficients at given pressure may be obtained by applying $\frac{d}{dP}$ to Eqs. (A1) or, for cubic crystals, directly to Eqs. (A2).

It should be noted that the B_{ijkl}'s have complete Voigt symmetry ($B_{\alpha\beta}$; $\alpha,\beta = \{1 \cdots 6\}$) only in the case of isotropic pressure [2,30].

APPENDIX B: EXPANSION OF EFFECTIVE ELASTIC CONSTANTS AROUND A ZERO PRESSURE CONFIGURATION

If a cubic material stays cubic under arbitrary pressure P, the effective elastic constants $B_{\alpha\beta}$ evaluated at this pressure may be expanded into a power series in terms of SOECs and TOECs *evaluated at the zero pressure configuration* and an expansion parameter ζ that measures the deformation from the zero pressure configuration to the loaded state, i.e., to first

order in ζ [2,30],

$$B_{11}(P) = C_{11} + \zeta[2(C_{11} + C_{12}) + C_{111} + 2C_{112}], \quad \text{(B1a)}$$

$$B_{12}(P) = C_{12} + \zeta[-(C_{11} + C_{12}) + C_{123} + 2C_{112}], \quad \text{(B1b)}$$

$$B_{44}(P) = C_{44} + \zeta[C_{44} + C_{11} + 2C_{12} + C_{144} + 2C_{166}]. \quad \text{(B1c)}$$

The relation between the expansion parameter and the pressure reads, for second order in P,

$$\zeta = -\frac{1}{m}P - \frac{n}{m^3}P^2, \quad \text{(B2)}$$

where

$$m = C_{11} + 2C_{12}, \quad \text{(B3)}$$

$$n = -(C_{11} + 2C_{12}) + \tfrac{1}{2}(C_{111} + 2C_{123} + 6C_{112}). \quad \text{(B4)}$$

Equation (B2) allows eliminating ζ in favor of P. The pressure derivatives of $B_{\alpha\beta}$ at $P = 0$ are readily obtained from Eqs. (B1) and (B2) and transformed into the pressure derivatives of the SOECs with the help of Eqs. (A2).

[1] Y. Hiki, Annu. Rev. Mater. Sci. **11**, 51 (1981).
[2] D. C. Wallace, *Thermoelastic Theory of Stressed Crystals and Higher-Order Elastic Constants* (Academic, New York, 1970), pp. 301–404.
[3] R. N. Thurston and K. Brugger, Phys. Rev. **133**, A1604 (1964).
[4] K. Brugger and T. C. Fritz, Phys. Rev. **157**, 524 (1967).
[5] M. Zoli, G. Santoro, V. Bortolani, A. A. Maradudin, and R. F. Wallis, Phys. Rev. B **41**, 7507 (1990).
[6] A. Gonzàlez-Comas and L. Mañosa, Phys. Rev. B **54**, 6007 (1996).
[7] B. P. Barua and S. K. Sinha, J. Appl. Phys. **49**, 3967 (1978).
[8] S. Chantasiriwan and F. Milstein, Phys. Rev. B **58**, 5996 (1998).
[9] X. Wang, Y. Gu, X. Sun, H. Wang, and Y. Zhang, J. Appl. Phys. **115**, 213516 (2014).
[10] Y. Hiki and A. V. Granato, Phys. Rev. **144**, 411 (1966).
[11] L. S. Cain and J. J. F. Thomas, Phys. Rev. B **8**, 5372 (1973).
[12] J. J. M. Lang and Y. M. Gupta, Phys. Rev. Lett. **106**, 125502 (2011).
[13] M. W. Riley and M. J. Skove, Phys. Rev. B **8**, 466 (1973).
[14] B. E. Powell and M. J. Skove, Phys. Rev. **174**, 977 (1968).
[15] P. N. Keating, Phys. Rev. **145**, 637 (1966).
[16] P. N. Keating, Phys. Rev. **149**, 674 (1966).
[17] T. Cağin and J. R. Ray, Phys. Rev. B **38**, 7940 (1988).
[18] J. Zhao, J. M. Winey, and Y. M. Gupta, Phys. Rev. B **75**, 094105 (2007).
[19] H. Wang and M. Li, Phys. Rev. B **79**, 224102 (2009).
[20] M. Łopuszyński and J. A. Majewski, Phys. Rev. B **76**, 045202 (2007).
[21] W. Pepperhoff and M. Acet, *Constitution and Magnetism of Iron and Its Alloys* (Springer, Berlin, 2010).
[22] D. J. Dever, J. Appl. Phys. **43**, 3293 (1972).
[23] X. Li, S. Schönecker, E. Simon, L. Bergqvist, H. Zhang, L. Szunyogh, J. Zhao, B. Johansson, and L. Vitos, Sci. Rep. **5**, 16654 (2015).
[24] H. Özkan and J. Jamieson, Phys. Chem. Miner. **2**, 215 (1978).
[25] A. M. Hofmeister and H. K. Mao, Proc. Natl. Acad. Sci. USA **99**, 559 (2002).
[26] T. Fuller and R. Brannon, Int. J. Eng. Sci. **49**, 311 (2011).
[27] O. Buck and G. A. Alers, *Fatigue and Microstructure* (American Society for Metals, Metals Park, Ohio, 1979).
[28] J. Kim, L. J. Jacobs, J. Qu, and J. W. Littles, J. Acoust. Soc. Am. **120**, 1266 (2006).
[29] G. E. Dace, R. B. Thompson, L. J. H. Brasche, D. K. Rehbein, and O. Buck, *Nonlinear Acoustics, a Technique to Determine Microstructural Changes in Materials*, (Springer-Plenum, New York, 1991).
[30] D. C. Wallace, Phys. Rev. **162**, 776 (1967).
[31] F. Birch, Phys. Rev. **71**, 809 (1947).
[32] T. H. K. Barron and M. L. Klein, Proc. Phys. Soc. **85**, 523 (1965).
[33] F. Birch, J. Geophys. Res. **83**, 1257 (1978).
[34] J. Wang, J. Li, S. Yip, S. Phillpot, and D. Wolf, Phys. Rev. B **52**, 12627 (1995).
[35] G. V. Sin'ko and N. A. Smirnov, J. Phys.: Condens. Matter **16**, 8101 (2004).
[36] R. Hill, Proc. Phys. Soc. London, Sect. A **65**, 349 (1952).
[37] J. H. Cantrell, J. Appl. Phys. **76**, 3372 (1961).
[38] R. Toupin and B. Bernstein, J. Acoust. Soc. Am. **33**, 216 (1961).
[39] K. Brugger, Phys. Rev. **133**, A1611 (1964).
[40] P. Hohenberg and W. Kohn, Phys. Rev. **136**, B864 (1964).
[41] J. P. Perdew, K. Burke, and M. Ernzerhof, Phys. Rev. Lett. **77**, 3865 (1996).
[42] O. K. Andersen, O. Jepsen, and G. Krier, in *Lectures on Methods of Electronic Structure Calculations*, edited by V. Kumar, O. K. Andersen, and A. Mookerjee (World Scientific, Singapore, 1994), p. 63.
[43] L. Vitos, H. L. Skriver, B. Johansson, and J. Kollár, Comput. Mater. Sci. **18**, 24 (2000).
[44] B. L. Gyorffy, Phys. Rev. B **5**, 2382 (1972).
[45] L. Vitos, I. A. Abrikosov, and B. Johansson, Phys. Rev. Lett. **87**, 156401 (2001).
[46] L. Vitos, *Computational Quantum Mechanics for Materials Engineers* (Springer-Verlag, London, 2007).
[47] L. Y. Tian, Q. M. Hu, R. Yang, J. Zhao, B. Johansson, and L. Vitos, J. Phys.: Condens. Matter **27**, 315702 (2015); L. Y. Tian, Licentiate thesis, Royal Institute of Technology, Sweden, 2015.
[48] H. Zhang, M. P. J. Punkkinen, B. Johansson, S. Hertzman, and L. Vitos, Phys. Rev. B **81**, 184105 (2010).
[49] X. Li, S. Schönecker, J. Zhao, B. Johansson, and L. Vitos, Phys. Rev. B **87**, 214203 (2013).
[50] L. Vitos, P. A. Korzhavyi, and B. Johansson, Nature Mater. **2**, 25 (2003).
[51] K. Koepernik and H. Eschrig, Phys. Rev. B **59**, 1743 (1999).
[52] G. Kresse and J. Furthmüller, Phys. Rev. B **54**, 11169 (1996).
[53] J. A. Rayne and B. S. Chandrasekhar, Phys. Rev. **122**, 1714 (1961).
[54] X. Li, H. Zhang, S. Lu, W. Li, J. Zhao, B. Johansson, and L. Vitos, Phys. Rev. B **86**, 014105 (2012).

[55] X. Li, S. Schönecker, J. Zhao, B. Johansson, and L. Vitos, J. Alloys Compd. **676**, 565 (2016).
[56] A. G. Every and A. K. McCurdy, *Low Frequency Properties of Dielectric Crystals Second and Higher Order Elastic Constants* (Springer, Berlin, 1992).
[57] H. Zhang, M. P. J. Punkkinen, B. Johansson, and L. Vitos, J. Phys.: Condens. Matter **22**, 275402 (2010).
[58] M. W. Guinan and D. N. Beshers, J. Phys. Chem. Solids **29**, 541 (1968).
[59] C. A. Rotter and C. S. Smith, J. Phys. Chem. Solids **27**, 267 (1966).
[60] F. F. Voronov and L. F. Vereshchagin, Phys. Met. Metallogr. **11**, 111 (1961).
[61] J. H. Cantrell and W. T. Yost, Int. J. Fatigue **23**, Suppl. 1, 487 (2001).
[62] K. H. Matlack, J. J. Wall, J.-Y. Kim, J. Qu, L. J. Jacobs, and H.-W. Viehrig, J. Appl. Phys. **111**, 054911 (2012).
[63] Z. Chen and J. Qu, J. Appl. Phys. **114**, 164906 (2013).